THE JOURNAL OF PHYSICAL CHEMISTRY C

Article

Cite This: J. Phys. Chem. C 2019, 123, 29418−29426

pubs.acs.org/JPCC

Nearly Isotropic Conjugated Polymer Aggregates with Efficient Local Exciton Diffusion

Youngah Kwon and Laura J. Kaufman*

Department of Chemistry, Columbia University, New York, New York 10027, United States

Supporting Information

ABSTRACT: To bridge the gap between single-molecule and bulk thin film studies of organic semiconductors and understand the influence of molecular structure on photophysical properties across scales, we prepared and characterized aggregates containing a few to more than a thousand single chains via well-controlled solvent vapor swelling of an inert polymeric matrix containing the conjugated polymer poly[2-methoxy-5-(2-ethylhexyloxy)-1,4-phenylenevinylene] (MEH-PPV). The single chains were initially immobilized in conformations with few interchain contacts, which can support exciton funneling on the single-molecule level. We show that aggregates prepared via solvent swelling and templated on such molecules result in largely isotropic aggregates. Analysis of aggregate polarization anisotropy, photoluminescence transient decay, and photoluminescence spectra as a function of aggregate size suggests that in these aggregates exciton diffusion is locally enhanced upon initial aggregation but does not reach extended length scales with further aggregation and annealing.

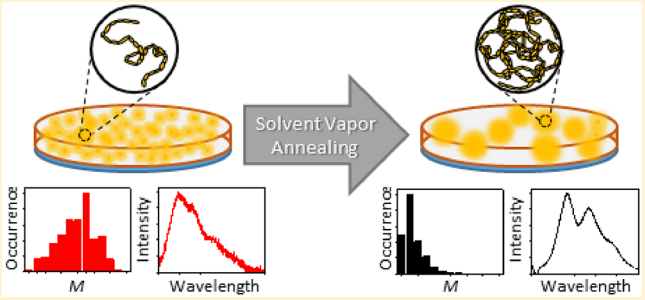

INTRODUCTION

Conjugated polymers have been extensively studied over the last two decades due to their potential as functional materials in optoelectronic devices including light-emitting diodes, solar cells, and photovoltaics.[1−9] Attractive qualities of conjugated polymers as components of such devices include their solution processability, mechanical properties, low production cost, and tunable photophysical properties. However, limitations exist, with conjugated polymer-based devices often suffering from limited device stability and low efficiency compared to their inorganic counterparts.[7,8] Some of these limitations are due to the nature of excitons, the fundamental excitations in conjugated polymers, which are Coulombically bound electron and hole pairs. While exciton migration is key to polymer-based device functionality, exciton migration to extrinsic impurities or intrinsic defects can lead to nonradiative or radiative recombination processes, either or both of which can inhibit desired device function.[10−16] Enhanced understanding and control of exciton behavior can lead to improvement in polymer-based device function, as highlighted by a recent paper in which a conjugated polymer electron donor layer was combined in a double-layered halide architecture.[17] Here, a wide bandgap halide was placed adjacent to a poly(3-hexylthiophene) [P3HT] electron donor layer to limit exciton recombination at the interface; this approach also induced ordered fibrillar morphology in the P3HT that encouraged hole transport, leading to exceptional efficiency for a solar cell employing a conjugated polymer layer.

The presence of multiple chromophores (a base unit for conjugation that consists of several monomers) as may exist on a single conjugated polymer assures complexity in exciton behavior and study thereof.[14,18−23] Interactions between chromophores determine the properties of conjugated polymers, including the efficiency and time scale of exciton migration. On a single-chain level, both intrachain (along-chain) and interchain (across-chain) processes can contribute to these properties. In the model conjugated polymer poly[2-methoxy-5-(2-ethylhexyloxy)-1,4-phenylenevinylene] (MEH-PPV), this leads to two distinct behaviors, which are linked to two distinct chain conformations. When dissolved in toluene, regarded as a poor solvent for MEH-PPV, and immobilized in an inert matrix such as poly(methyl methacrylate) or polystyrene, MEH-PPV chains are known to adopt a collapsed and ordered conformation, as supported by evidence of highly aligned transition dipoles in experiments and simulation.[14,24−31] These molecules show stepwise photobleaching and relatively red emission, providing evidence that the chain planarization and/or interchain interactions predominant in MEH-PPV chains with such conformations support relatively long conjugation lengths and facile exciton migration.[14,32−38] Alternately, when dissolved in chloroform, MEH-PPV chains adopt a random coil conformation in which intrachain interactions dominate. In this case, the MEH-PPV chains typically show low polarization anisotropy, continuous photobleaching, and higher energy emission.[14,26,32,33,35,39−42]

Received: August 23, 2019
Revised: October 23, 2019
Published: November 11, 2019

DOI: 10.1021/acs.jpcc.9b08075
J. Phys. Chem. C 2019, 123, 29418−29426

Though on a single-molecule level the relationship between conformation and photophysical properties has largely been elucidated, the full array of interactions present in densely packed environments such as those in devices cannot be fully recapitulated at the single-molecule level. To enhance understanding of the relationship between conjugated polymer conformation and photophysics, as well as to bridge single-molecule and bulk level studies, aggregates and nanoparticles of conjugated polymers have been the subject of recent work.[27,43−53] It is particularly instructive to study aggregates prepared in a controlled and reproducible manner, and, as such, aggregates have been prepared through solvent vapor swelling of a host polymer matrix containing the conjugated polymer chains of interest.[49] The swelling invoked by the solvent vapor introduced to the system allows for conjugated polymer chain diffusion and aggregation via Ostwald ripening and/or particle coalescence.[46]

Here, we use a multimodal apparatus previously described that affords control over the aggregation process and simultaneous wide-field fluorescence imaging[54] to characterize aggregates of MEH-PPV in PMMA. In contrast to our previous work focused on MEH-PPV initially dissolved in toluene,[45] which supports a collapsed and ordered conformation, here we study MEH-PPV initially dissolved in chloroform, which supports the random coil conformation at the single-molecule level. We show that the relatively isotropic conformation of single MEH-PPV chains following dissolution in chloroform is maintained even after solvent vapor annealing and multichain aggregation. Previous studies have explored the effects of conjugated polymer conformation at the single-molecule level on aggregate structure and photophysics, but those studies controlled single-molecule conformation by controlling regio-regularity or introducing defects or halogen atoms during polymer synthesis.[43,44,50] Here, we show that even a change in dissolving solvent during sample preparation impacts aggregate physical conformation and photophysical behavior despite swelling of the background matrix that allows conjugated polymer mobility. In these systems, we find indications of local enhancement of interchain interactions due to aggregation (red shift of emission spectra and increasing quenching efficiency) without signs of long-range exciton migration that were apparent in aggregates templated on MEH-PPV molecules with collapsed and ordered conformation.[45] This work provides insights into the complex relationship between polymer morphology and energy transfer, adding to the set of findings suggesting the importance of sample preparation in setting exciton migratory capacity in conjugated polymers across scales.[31,43,50,55−58]

METHODS

Sample Preparation. MEH-PPV (M_w = 168 kDa and PDI = 2.1) was synthesized as described previously.[59] Poly(methyl methacrylate) (PMMA; M_w = 97 kDa and PDI = 2.2) was purchased from Sigma-Aldrich and purified before use.[60] MEH-PPV solutions of four different concentrations—concentrations A, B, C, and D—were prepared by dissolving MEH-PPV in chloroform (HPLC plus grade), which was purchased from Sigma-Aldrich and used without further purification. Concentration A was ~10^{-11} M, and concentrations B, C, and D were 10, 100, and 1000 times concentration A, respectively. The prepared MEH-PPV solutions were then mixed with ~2.5 wt % PMMA/chloroform solution at a 1:500 ratio, so that the final concentration A was a typical concentration used for single-molecule studies. Spin-coating was used to deposit the solutions onto piranha-cleaned glass coverslips, which resulted in emissive feature density of ~0.4 spots/μm^3.

Solvent Vapor Annealing (SVA). The SVA technique employed is described in detail elsewhere.[54] Briefly, a solvent reservoir, a mixing bottle, and three mass flow controllers (MFCs; Alicat Scientific, two MCS-100SCCMs and one MCS-200SCCM) were used to control the solvent vapor flow of the system. First, dry N_2 gas was introduced to the solvent reservoir through an MFC where the flow rate was controlled. The solvent vapor was generated by bubbling the N_2 gas in the solvent reservoir. A mixture of chloroform and acetone (50:50 liquid volume ratio; 43.7:56.3 vapor ratio) was used. The solvent vapor entered the mixing bottle, where more N_2 gas could be introduced through two additional MFCs if needed. The solvent vapor then traveled to the SVA chamber where two films were placed, one deposited on a glass coverslip, used for wide-field fluorescence measurements, and one on a quartz crystal microbalance (QCM) sensor, used for monitoring the SVA process. The QCM (Stanford Research Systems, QCM-200) detected mass change of the film, which was converted to changes in film thickness. The initial thickness of sample films was 210 ± 5 nm, and during SVA, unless otherwise specified, the swollen film thickness was 535 ± 5 nm, which was controlled through N_2 flow into the solvent reservoir that in turn controls the solvent vapor flow rate, adjusting the MFC as needed for the duration of swelling. Except when otherwise noted, films were swollen for 50 min and then deswelled by flowing dry N_2 gas into the SVA chamber. All experiments were carried out at room temperature (21 °C).

Wide-Field Epifluorescence Imaging. A continuous-wave 488 nm diode laser (Thorlabs, L488P60) was used as the excitation source. It was coupled to a multimode fiber that was mechanically shaken to improve homogeneity of the illumination. A linear polarizer and a quarter-wave plate were used to generate circularly polarized light. The beam then passed through a laser line filter and a collimating lens, reflected off a dichroic mirror, and was focused onto the back-focal plane of an oil-immersion objective (Olympus PlanApo N 60×, NA = 1.45). For polarization modulation measurements, a motorized rotating linear polarizer was placed before the dichroic mirror and rotated at 10°/s. The fluorescence from the sample was collected with the same objective and was filtered using a 514 nm long-pass filter before imaging onto an EMCCD camera (Andor, iXon DV885 KCS-VP). The 14-bit images were recorded over 512 pixels × 512 pixels. The final field of view was 47 μm × 47 μm. All fluorescent features were first identified using the Crocker-Grier algorithm via the Trackpy Python toolkit. The intensities of identified features were then calculated and background-corrected using a custom program written in Python. In short, the pixel intensities of the identified feature area were summed; then, the median pixel intensity of the entire field-of-view (representing background intensity) was multiplied by the number of pixels in the feature area, and this background value was subtracted from the summed feature intensity. Details of the calculation are presented in ref 45.

To collect photoluminescence spectra, a spectrograph (Andor Shamrock 193i) was placed before the EMCCD camera. When collecting spectra, a 498 nm long-pass filter was used in place of the 514 nm filter, and the 14-bit images were recorded over 1002 × 1004 pixels. All spectra were fit to three

DOI: 10.1021/acs.jpcc.9b08075
J. Phys. Chem. C 2019, 123, 29418−29426

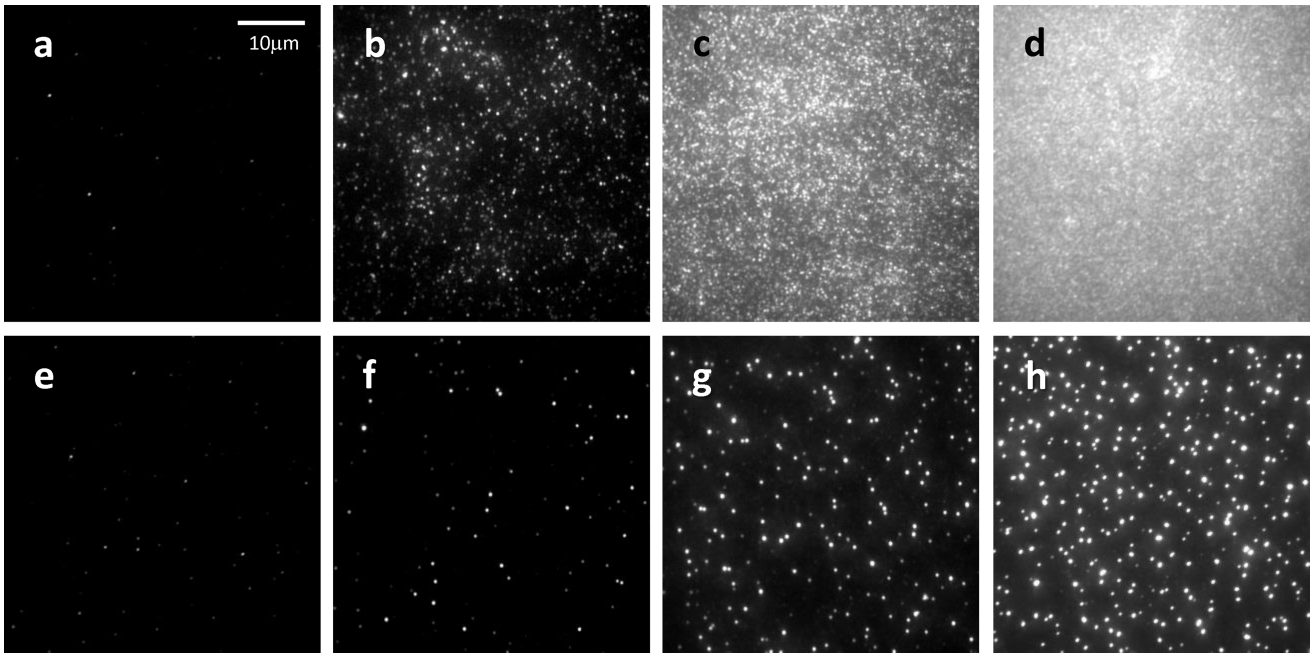

Figure 1. Representative wide-field fluorescence images of films of concentrations A–D (a–d) before and (e–h) after SVA. Intensity scale for the images is 1100–1500, 1100–2550, and 1100–10000 counts per 200 ms for films of concentrations A and B, C, and D, respectively. Excitation power density was 2.5 W/cm^2 for all films.

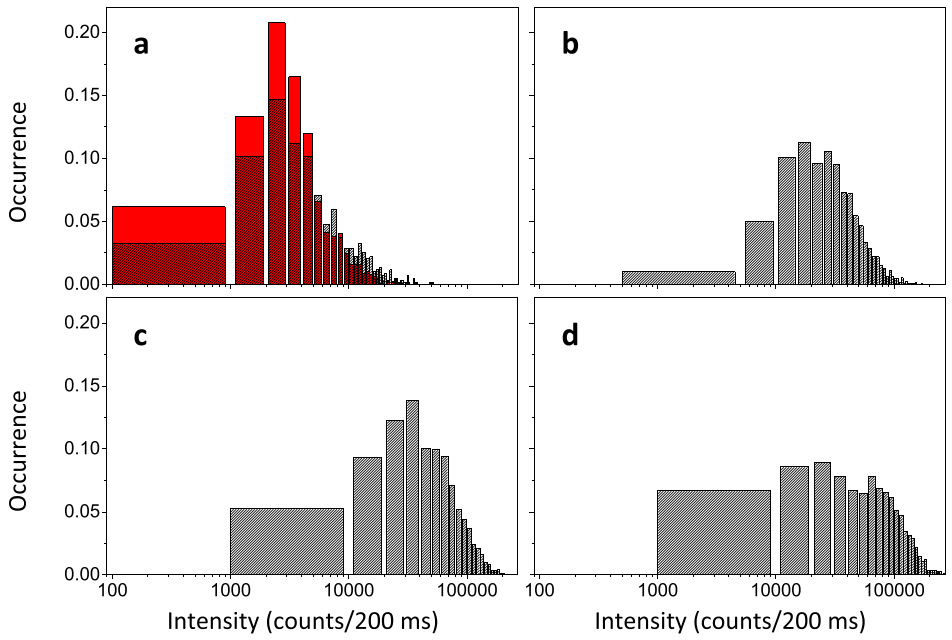

Figure 2. Histograms of fluorescence intensity of identified features in (a) concentration A (red) before and (black) after SVA and (b–d) concentrations B–D after SVA. The median intensities are 3 500, 5 090, 31 500, 49 200, and 66 000 counts per 200 ms at 5 W/cm^2, respectively. Measurements were taken over at least 5 fields, and total number of features represented by the histograms are 890, 591, 1692, 1621, and 1108 for films of concentration A before SVA and after SVA and for films of concentrations B–D after SVA, respectively. Histograms are normalized by total area.

Gaussian or Voigt functions via least-squares fitting except as noted. Peak positions and relative heights were determined from the sum of the deconvolved spectra, which is the reconstructed spectrum without noise, except where noted.

RESULTS AND DISCUSSION

Wide-field fluorescence images were collected before and after SVA for sample films of concentrations A–D (Figure 1). In films of concentrations A and B, individual bright features on a dark background are evident before SVA, and the number of such features decreases after SVA, with this change quite subtle in films of concentration A and quite obvious in films of concentration B. For films of concentrations C and D, a bright background exists due to the large number of single molecules present that result in overlapping imaged features. In these samples, fluorescence intensity of the background of the films

DOI: 10.1021/acs.jpcc.9b08075
J. Phys. Chem. C 2019, 123, 29418–29426

decreases significantly after SVA, and the intensity of the clearly identifiable features increases. Taken together, this suggests that in samples B−D, single molecules aggregate to form multichain entities as a result of SVA. From here forward, we denote these features as aggregates B−D. Figure 2 shows the fluorescence intensity histograms of identified features of sample films before and after SVA for concentration A and after SVA for concentrations B−D. Fluorescence intensity of bright features following SVA increases as a function of initial MEH-PPV concentration, suggesting that at higher initial concentrations, larger aggregates are formed.

To assess conformation, polarization modulation depth (M) measurements of single MEH-PPV molecules and/or aggregates were performed. M was obtained by rotating a linear polarizer while collecting fluorescence images. Fluorescence intensities of MEH-PPV particles were plotted as a function of polarization angle and fit to the function $I(\phi) = I_0[1 + M_{COS}\{2(\phi - \phi_0)\}]$, where ϕ is polarization angle, ϕ_0 is a reference polarization angle at the intensity maximum, and I_0 is a reference fluorescence intensity at the intensity maximum. M values report the alignment of absorbing transition dipoles and thus report on the conformation of MEH-PPV molecules or aggregates, with M near 1 for molecules or aggregates with highly aligned chromophores and close to 0 for isotropic chromophore arrangement. Excitation power densities were 7.5, 1.0, 0.5, and 0.5 W/cm^2 for concentration A before and after SVA and concentrations B, C, and D after SVA, respectively. This power is low enough to avoid potential M value suppression due to exciton−exciton annihilation[61,62] as well as to suppress potential variation in signal from MEH-PPV molecules remaining in the background.[45]

The histogram of single-molecule M values before SVA shown in Figure 3a shows a median value of 0.66, in close agreement with previous results for MEH-PPV single molecules initially dissolved in chloroform.[26] We note that

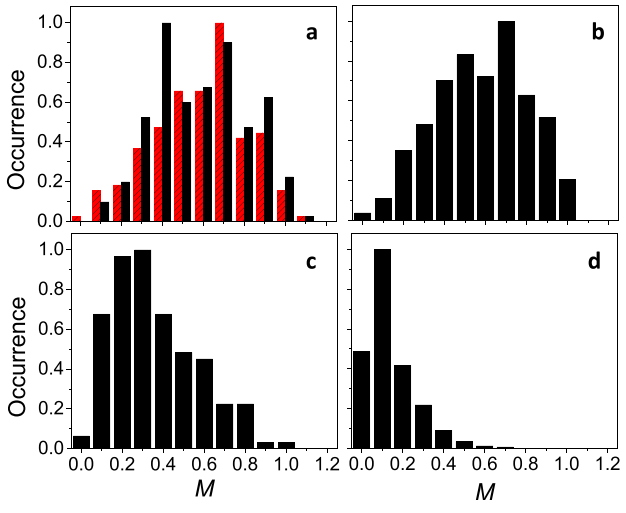

Figure 3. Histograms of polarization modulation depth (M) of features identified in (a) films of concentration A (red) before and (black) after SVA and (b−d) films of concentrations B−D after SVA. The median M values are 0.66, 0.64, 0.63, 0.37, and 0.16, respectively, for concentration A before and after SVA and aggregates B−D. Measurements are taken over at least 3 fields, and total number of features represented by the histograms are 174, 214, 302, 150, and 321 for films of concentration A before SVA and after SVA as well as for films of concentrations B−D after SVA, respectively.

sample A shows little change in median M value after SVA (median M = 0.64). Despite the fact that this sample was sufficiently swollen to allow obvious molecular mobility, the single molecules apparently adopted similar conformations after SVA as that displayed following initial sample preparation through spin-coating. This stands in contrast to a previous study in which MEH-PPV was dissolved in chloroform and swollen in toluene vapor, in which the M values shifted to higher values signaling molecular collapse and ordering.[26] In the current work, swelling was performed in a combination of chloroform and acetone, and while acetone has been reasoned to be a poor solvent for MEH-PPV owing to its high polarity, in combination with chloroform it apparently does not induce the collapsed, ordered conformation. Given the consistency of M measurements before and after SVA for films of concentration A, presumably the template for aggregate formation is a poorly ordered, loosely arranged MEH-PPV molecule. This is consistent with findings for polarization modulation values in aggregates B−D. Aggregates B show little shift from the single-molecule M distribution, while for the larger aggregates, decrease in M values is apparent, with median values decreasing from the single-molecule value of 0.66 to 0.37 and 0.16 for aggregates C and D, respectively. This is in contrast to large aggregates initially templated on the collapsed, ordered single molecules prepared in toluene, where aggregates with several hundred molecules showed M distributions peaked above 0.60.[45] While the M distributions of the aggregates prepared in this study are indicative of largely isotropic aggregates, we note that these values are still higher than would be expected from large aggregates with fully randomized transition dipole orientation.[42]

To characterize additional aspects of the photophysical behavior of MEH-PPV aggregates, fluorescence intensity transients were collected, with representative plots shown in Figure 4. To encourage photobleaching, the transients were collected using a high excitation power density of 200 W/cm^2. Some intensity transients in samples of concentration A before and after SVA show stepwise photobleaching, but many show relatively smooth decays, as shown in Figure 4a and consistent with previous measurements of MEH-PPV single molecules dissolved in chloroform, and with the latter behavior associated with intramolecular exciton transport interrupted by many recombination events.[32,33,35] The lack of distinct photoblinking and photobleaching events is also seen in aggregates B−D (Figure 4b−d). This behavior is again in contrast to MEH-PPV aggregates formed from molecules initially dissolved in toluene, where distinct steps in fluorescence transients were apparent in aggregates comprised of up to several hundred MEH-PPV chains.[45]

To further characterize the photophysics of the MEH-PPV aggregates, photoluminescence spectra were collected. In Figure 5a, representative individual and average spectra of single molecules of MEH-PPV dissolved in chloroform and dispersed in PMMA before SVA are shown. As described previously for molecules of similar molecular weight following dissolution in chloroform and immobilization in a polymer matrix, the individual spectra are generally broad, with many molecules showing a 0−0 peak near 545 nm and a second peak near 580 nm.[32] A few molecules display a somewhat red-shifted spectrum, with 0−0 peak near 570 nm. Spectra of the features found following SVA are distinct from those before SVA, with increased homogeneity across features and somewhat narrower spectral bands (Figure 5b). These features have

DOI: 10.1021/acs.jpcc.9b08075
J. Phys. Chem. C 2019, 123, 29418−29426

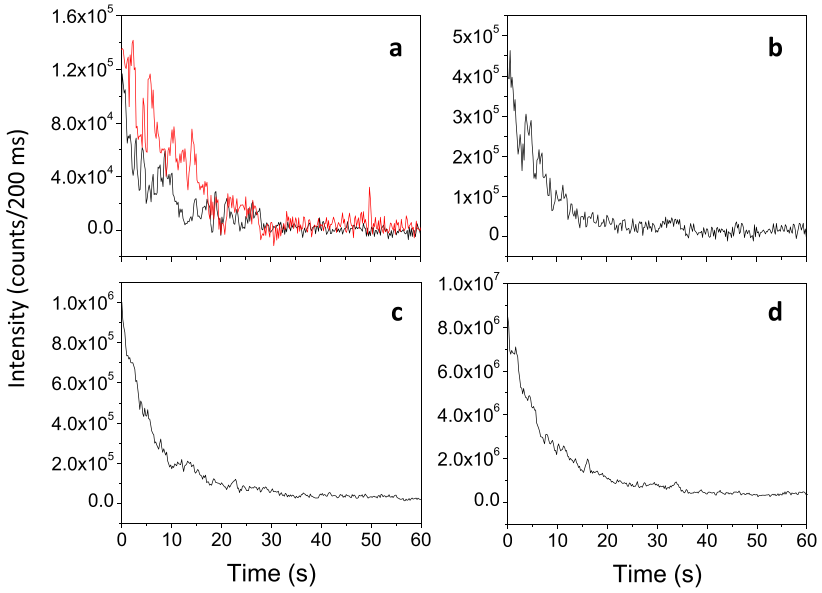

Figure 4. Representative fluorescence intensity transients of features found in (a) films of concentration A (red) before and (black) after SVA and (b–d) aggregates B–D.

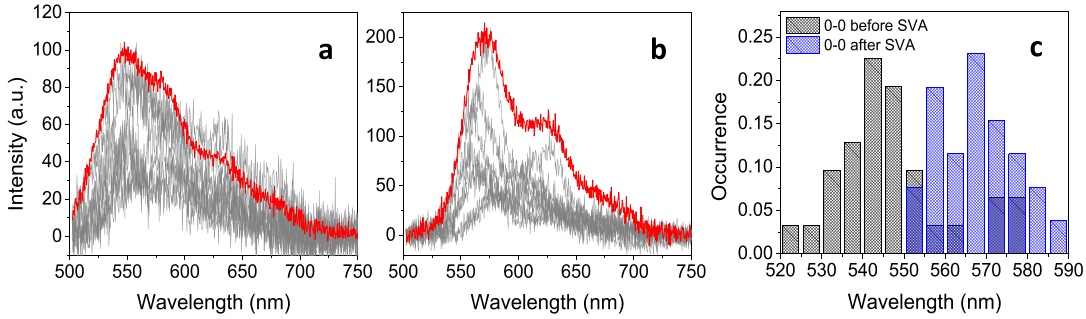

Figure 5. (a, b) Eight representative (gray) individual spectra and (red) the average spectrum of MEH-PPV features found in films of concentration A (a) before and (b) after SVA. Average spectra are obtained from 23 and 26 individual spectra before and after SVA, respectively. (c) Histograms of 0–0 peak positions of MEH-PPV features before and after SVA.

notably red-shifted spectra relative to features found before SVA, with the median peak position of the 0–0 and 0–1 peaks at ∼570 (Figure 5c) and 625 nm, respectively. Such spectra have previously been associated with relatively large MEH-PPV molecules exhibiting collapsed conformations[32,63−67] as well as with tightly packed aggregates;[47,50,68,69] in both cases, chain planarization, $\pi-\pi$ stacking, and extension of effective conjugation length can occur, potentially allowing excitons to efficiently funnel to red sites through interchain or intermolecular contacts. In particular, the shifts seen between spectra obtained from films of concentration A before and after SVA are quite similar to those seen previously when single molecules of MEH-PPV were dissolved in tetrahydrofuran (THF), a good solvent for MEH-PPV, and interrogated first at the single-molecule level and then following aggregation to 10–100 nm nanoparticles formed via reprecipitation through rapid addition of water to MEH-PPV in THF solution.[47]

While such a shift toward lower energy emission is consistent with aggregation, it is also consistent with molecular collapse. While no shift in the distribution of M values before and after SVA in films of concentration A that would point to collapse was apparent, to clarify whether the spectral shift was due to conformational change or to the formation of small aggregates, samples of concentration A were prepared and subjected to a degree and time of swelling expected to allow for conformational change but that did not result in obvious translational diffusion. For this experiment, 10 min of SVA was performed using the same mixture of chloroform and acetone used in all other measurements. Swelling was held to approximately one-third of that of the typical experiments, with average swollen film thickness of ∼300 vs 535 nm. This experiment showed no change in spectra before and after SVA (Figure S1). This supports the idea that the spectral change observed in films of concentration A before and after SVA is not due to conformational change in the single molecules but instead to aggregation.

For films of concentration A, features are well separated and distinct both before and after SVA, and the background level between those features is consistent with that of the pure host polymer matrix alone. As such, feature-finding is an appropriate way to characterize number of molecules per aggregate following SVA. Over five fields of view, before SVA, 233 ± 50 features, assumed to be single molecules, as supported by the spectra, were found; after SVA, 149 ± 9 features were found. This suggests approximately two molecules are present per feature following solvent vapor annealing. Interestingly, the increase in homogeneity and red shift seen before and after SVA occurs even with this very small degree of aggregation.

DOI: 10.1021/acs.jpcc.9b08075
J. Phys. Chem. C 2019, 123, 29418−29426

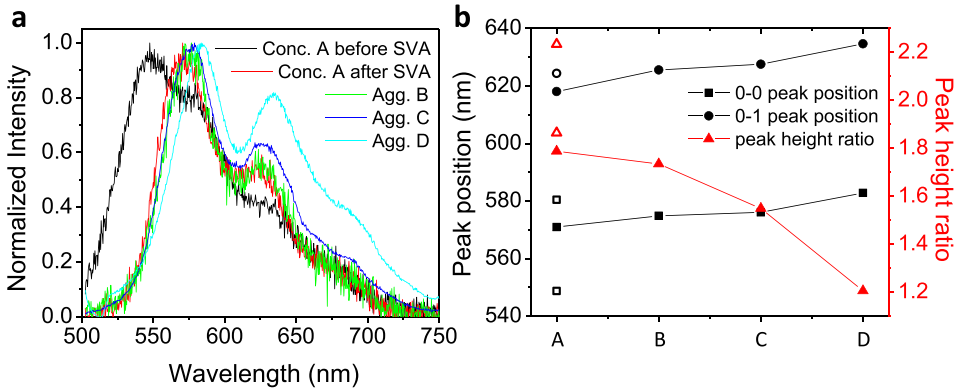

Figure 6. (a) Ensemble-averaged spectra of MEH-PPV in films of concentration A before and after solvent vapor annealing as well as of aggregates B–D. The excitation power densities used were 280, 280, 330, and 88.7 W/cm^2, for films of concentrations A–D, respectively. Spectra for concentration A are also shown in Figure 5a. Number of individual spectra averaged for aggregates B–D are 9, 12, and 7, respectively. (b) (Black squares) 0–0 peak position, (black circles) 0–1 peak position, and (red triangles) 0–0/0–1 peak height ratios for features in films of concentration A–D as obtained from average spectra shown in (a). The results for concentration A before SVA are shown as open symbols. This spectrum was fit with four Gaussian functions: the two squares show the positions of the first two peaks, and the open circle indicates the position of the third peak. Peak ratios between the first and third and the second and third peaks are shown as open triangles. Peak position and peak height ratio for individual spectra after SVA that contribute to the average spectra shown and evaluated here are shown in Figure S2.

We next investigated the spectra of aggregates formed following SVA of films of concentrations B–D. Peak positions in the aggregates shift to the red with increasing size, with 0–0 and 0–1 peak positions shifting from 572 to 584 and from 623 to 635 for aggregates A–D, respectively (Figure 6). The relative height of the 0–0 and 0–1 peaks also evolves from aggregates A through D, decreasing as a function of aggregate size (Figure 6b).

The changes in aggregate spectra as a function of initial film concentration prompted analysis of number of molecules per aggregate, $N_{SM\text{-}AGG}$. While this quantity in films of concentration A was assessed using a feature-finding approach as described above, to characterize aggregate size in films of higher concentrations, we used an approach similar to one we devised previously[45] as described in the Supporting Information: this approach (1) does not require that all features be identified and counted before SVA, as becomes increasingly difficult at high initial film concentration, and (2) does not assume aggregate intensity reports directly on number of single chains in aggregates, since quenching phenomena are known to occur upon aggregation.[51] Instead, this approach uses background film intensity after SVA to characterize the number of molecules remaining in the background and the number of aggregates present after SVA to calculate the number of molecules present, on average, in each aggregate. This approach assumes that intensity emerging from the background of the samples is due to single-molecule emission. However, spectra obtained from the background of such samples following SVA suggested this was not a good assumption for films of concentration C and D, as here spectra from the film in locations with no obvious aggregates following SVA showed spectral features consistent with aggregates rather than single molecules (Figure S3). With this in mind (see the Supporting Information), the number of single molecules per aggregate, $N_{SM\text{-}AGG}$, was calculated, yielding $N_{SM\text{-}AGG}$ = 30 ± 5, 255 ± 11, and 1640 ± 69 molecules per aggregate for aggregates B–D, respectively. Comparing the number of molecules per aggregate with the intensities per aggregate (Figure 1), it is clear that intensity does not scale linearly with number of molecules and quenching is strong in the aggregates formed here, with quenching efficiency increasing with aggregate size, the same trend that was found in the toluene-prepared aggregates in our previous publication.[45]

Taking together information obtained from M measurements, intensity transients, and spectra in both single MEH-PPV molecules and aggregates, a seeming juxtaposition emerges. M distributions show relatively low anisotropy at both the single-molecule and aggregate level, with aggregates of increasing size showing strongly decreasing median M values, especially compared to aggregates formed in toluene.[45] This suggests aggregation is occurring not in a manner that leads to compaction and ordering but instead in a manner that inhibits formation of a large number of new intermolecular contacts that support exciton funneling to low-energy sites. This is consistent with smoothly decreasing intensity transients that point to interruption of such potential exciton funneling with large numbers of (relatively low-intensity) radiative events. In contrast, a strong red spectral shift is seen following SVA, suggesting that exciton funneling to low-energy sites is occurring. The fact that such a spectral shift happens already upon aggregation of just a few molecules (aggregate A) with little additional spectral peak position evolution upon further aggregation suggests this spectral shift reflects local effects that do not extend across larger aggregates, in contrast to findings in toluene-prepared aggregates. This is also supported by the decrease of the 0–0/0–1 peak ratio as a function of increasing aggregate size, consistent with interchain coupling in the presence of disorder, as captured by the description of MEH-PPV aggregates as strongly disordered HJ-aggregates.[38,70] Similarly, increasing quenching efficiency as a function of aggregate size need not indicate efficient packing through intermolecular contacts that facilitate exciton transport, as such quenching, which reflects new nonradiative pathways available, may also be local in nature. This is consistent with an earlier finding showing that MEH-PPV aggregate coalescence, a process that diminishes order in the aggregates and is suggested to occur through a point and at random orientation, also leads to quenching.[46]

Finally, it is interesting to note that while the most notable spectral changes occur between single molecules and small aggregates A, spectral shift continues as a function of aggregate

DOI: 10.1021/acs.jpcc.9b08075
J. Phys. Chem. C 2019, 123, 29418–29426

size, evolving even between aggregates C and D, with the spectrum of aggregate D quite similar to spectra of thin films of MEH-PPV, with reported 0−0 peak positions of ∼585 nm.[71,72] The additional red shift, together with decrease in the 0−0/0−1 peak ratio, between aggregates C and D indicates a transition from individual aggregate to bulk film properties between aggregates of several hundred chains and those of over a thousand single chains for the preparation conditions used here, which include initial dissolution in a good solvent followed by swelling in a mix of solvents that supports a combination of Ostwald ripening, shown in some contexts to support chain ordering, and coalescence, shown to limit photophysical anisotropy and exciton diffusion.[27,46]

CONCLUSIONS

This study demonstrates self-assembly of largely isotropic aggregates of MEH-PPV via controlled and reproducible solvent vapor swelling of an inert polymer matrix seeded with dispersed single MEH-PPV chains. Polarization modulation histograms indicate that aggregates templated on molecules initially showing low compaction and limited transition dipole alignment maintain those characteristics even when the single-molecule conformation is set only by choice of initial dissolving solvent. The poor compaction of the aggregate limits enhancement of exciton diffusion in these aggregates relative to single molecules, as reflected in fluorescence transients that do not show evidence of long length scale exciton diffusion. However, sufficient new intermolecular interactions emerge to red shift the spectrum of aggregates relative to single molecules, with aggregates comprised of just a few molecules already showing notable spectral changes relative to isolated molecules. Aggregates composed of few to more than a thousand single molecules show additional spectral evolution as a function of aggregate size, both red shifting and showing a decreased ratio of 0−0 to 0−1 peak intensities. Taken together, these results suggest locally enhanced exciton diffusion upon aggregation of a few molecules but limited enhancement of that effect upon further aggregation, as ordering that occurs in few molecule aggregates does not extend over longer distances and larger structures.

ASSOCIATED CONTENT

Supporting Information

The Supporting Information is available free of charge at https://pubs.acs.org/doi/10.1021/acs.jpcc.9b08075.

Detailed information on the calculation of number of single molecules per aggregate; spectra of features before and after limited SVA (Figure S1); individual spectrum characteristics for aggregates described also by Figure 6 (Figure S2); spectra and spectral characteristics of the film background following SVA for films of concentrations C and D (Figure S3) (PDF)

AUTHOR INFORMATION

Corresponding Author

*E-mail: kaufman@chem.columbia.edu.

ORCID

Laura J. Kaufman: 0000-0002-3754-0831

Notes

The authors declare no competing financial interest.

ACKNOWLEDGMENTS

We thank Jaesung Yang for helpful discussions. This work was supported by NSF CHE 1807931.

REFERENCES

(1) Friend, R. H.; Gymer, R. W.; Holmes, A. B.; Burroughes, J. H.; Marks, R. N.; Taliani, C.; Bradley, D. D. C.; Dos Santos, D. A.; Brédas, J.-L.; Logdlund, M.; Salaneck, W. R.; et al. Electroluminescence in Conjugated Polymers. *Nature* **1999**, *397*, 121−128.

(2) Zheng, H.; Zheng, Y.; Liu, N.; Ai, N.; Wang, Q.; Wu, S.; Zhou, J.; Hu, D.; Yu, S.; Han, S.; et al. All-Solution Processed Polymer Light-Emitting Diode Displays. *Nat. Commun.* **2013**, *4*, 1971.

(3) Kaake, L. G.; Barbara, P. F.; Zhu, X. Intrinsic Charge Trapping in Organic and Polymeric Semiconductors: A Physical Chemistry Perspective. *J. Phys. Chem. Lett.* **2010**, *1*, 628−635.

(4) Günes, S.; Neugebauer, H.; Sariciftci, N. S. Conjugated Polymer-Based Organic Solar Cells. *Chem. Rev.* **2007**, *107*, 1324−1338.

(5) Coakley, K. M.; McGehee, M. D. Conjugated Polymer Photovoltaic Cells. *Chem. Mater.* **2004**, *16*, 4533−4542.

(6) Lu, L.; Yu, L. Understanding Low Bandgap Polymer PTB7 and Optimizing Polymer Solar Cells Based on It. *Adv. Mater.* **2014**, *26*, 4413−4430.

(7) Yu, L.; Liang, Y. A New Class of Semiconducting Polymers for Bulk Heterojunction Solar Cells with Exceptionally High Performance. *Acc. Chem. Res.* **2010**, *43*, 1227−1236.

(8) Hou, W.; Xiao, Y.; Han, G.; Lin, J. Y. The Applications of Polymers in Solar Cells: A Review. *Polymers (Basel, Switz.)* **2019**, *11*, 143.

(9) Yang, J.; Zhao, Z.; Wang, S.; Guo, Y.; Liu, Y. Insight into High-Performance Conjugated Polymers for Organic Field-Effect Transistors. *Chem.* **2018**, *4*, 2748−2785.

(10) Bardeen, C. J. Exciton Quenching and Migration in Single Conjugated Polymers. *Science* **2011**, *331*, 544−545.

(11) Rothberg, L. J.; Yan, M.; Papadimitrakopoulos, F.; Galvin, M. E.; Kwock, E. W.; Miller, T. M. Photophysics of Phenylenevinylene Polymers. *Synth. Met.* **1996**, *80*, 41−58.

(12) Vanden Bout, D. A.; Yip, W.-T.; Hu, D.; Fu, D.-K.; Swager, T. M.; Barbara, P. F. Discrete Intensity Jumps and Intramolecular Electronic Energy Transfer in the Spectroscopy of Single Conjugated Polymer Molecules. *Science* **1997**, *277*, 1074−1077.

(13) Adachi, T.; Vogelsang, J.; Lupton, J. M. Unraveling the Electronic Heterogeneity of Charge Traps in Conjugated Polymers by Single-Molecule Spectroscopy. *J. Phys. Chem. Lett.* **2014**, *5*, 573−577.

(14) Lupton, J. M. Single-Molecule Spectroscopy for Plastic Electronics: Materials Analysis from the Bottom-Up. *Adv. Mater.* **2010**, *22*, 1689−1721.

(15) Mikhnenko, O. V.; Blom, P. W. M.; Nguyen, T. Q. Exciton Diffusion in Organic Semiconductors. *Energy Environ. Sci.* **2015**, *8*, 1867−1888.

(16) Lee, H.; Park, C.; Sin, D. H.; Park, J. H.; Cho, K. Recent Advances in Morphology Optimization for Organic Photovoltaics. *Adv. Mater.* **2018**, *30*, 1800453.

(17) Jung, E. H.; Jeon, N. J.; Park, E. Y.; Moon, C. S.; Shin, T. J.; Yang, T. Y.; Noh, J. H.; Seo, J. Efficient, Stable and Scalable Perovskite Solar Cells Using Poly(3-Hexylthiophene). *Nature* **2019**, *567*, 511−515.

(18) Lupton, J. M. Chromophores in Conjugated Polymers - All Straight? *ChemPhysChem* **2012**, *13*, 901−907.

(19) Schindler, F.; Jacob, J.; Grimsdale, A. C.; Scherf, U.; Müllen, K.; Lupton, J. M.; Feldmann, J. Counting Chromophores in Conjugated Polymers. *Angew. Chem., Int. Ed.* **2005**, *44*, 1520−1525.

(20) Schwartz, B. J. Conjugated Polymers: What Makes a Chromophore? *Nat. Mater.* **2008**, *7*, 427−428.

(21) Becker, K.; Da Como, E.; Feldmann, J.; Scheliga, F.; Csányi, E. T.; Tretiak, S.; Lupton, J. M. How Chromophore Shape Determines the Spectroscopy of Phenylene-Vinylenes: Origin of Spectral Broadening in the Absence of Aggregation. *J. Phys. Chem. B* **2008**, *112*, 4859−4864.

DOI: 10.1021/acs.jpcc.9b08075
J. Phys. Chem. C 2019, 123, 29418−29426

(22) Traub, M. C.; Dubay, K. H.; Ingle, S. E.; Zhu, X.; Plunkett, K. N.; Reichman, D. R.; Vanden Bout, D. A. Chromophore-Controlled Self-Assembly of Highly Ordered Polymer Nanostructures. *J. Phys. Chem. Lett.* **2013**, *4*, 2520−2524.
(23) Schindler, F.; Lupton, J. M. Single Chromophore Spectroscopy of MEH-PPV: Homing-in on the Elementary Emissive Species in Conjugated Polymers. *ChemPhysChem* **2005**, *6*, 926−934.
(24) Adachi, T.; Brazard, J.; Chokshi, P.; Bolinger, J. C.; Ganesan, V.; Barbara, P. F. Highly Ordered Single Conjugated Polymer Chain Rod Morphologies. *J. Phys. Chem. C* **2010**, *114*, 20896−20902.
(25) Ebihara, Y.; Vacha, M. Relating Conformation and Photophysics in Single MEH-PPV Chains. *J. Phys. Chem. B* **2008**, *112*, 12575−12578.
(26) Vogelsang, J.; Brazard, J.; Adachi, T.; Bolinger, J. C.; Barbara, P. F. Watching the Annealing Process One Polymer Chain at a Time. *Angew. Chem., Int. Ed.* **2011**, *50*, 2257−2261.
(27) Vogelsang, J.; Adachi, T.; Brazard, J.; Vanden Bout, D. A.; Barbara, P. F. Self-Assembly of Highly Ordered Conjugated Polymer Aggregates with Long-Range Energy Transfer. *Nat. Mater.* **2011**, *10*, 942−946.
(28) Hu, D.; Yu, J.; Wong, K.; Bagchi, B.; Barbara, P. F.; Rossky, P. J. Collapse of Stiff Conjugated Polymers with Chemical Defects into Ordered, Cylindrical Conformations. *Nature* **2000**, *405*, 1030−1033.
(29) Hu, D.; Yu, J.; Barbara, P. F. Single-Molecule Spectroscopy of the Conjugated Polymer MEH-PPV. *J. Am. Chem. Soc.* **1999**, *121*, 6936−6937.
(30) Bounos, G.; Ghosh, S.; Lee, A. K.; Plunkett, K. N.; Dubay, K. H.; Bolinger, J. C.; Zhang, R.; Friesner, R. A.; Nuckolls, C.; Reichman, D. R.; et al. Controlling Chain Conformation in Conjugated Polymers Using Defect Inclusion Strategies. *J. Am. Chem. Soc.* **2011**, *133*, 10155−10160.
(31) Traub, M. C.; Lakhwani, G.; Bolinger, J. C.; Vanden Bout, D. A.; Barbara, P. F. Electronic Energy Transfer in Highly Aligned MEH-PPV Single Chains. *J. Phys. Chem. B* **2011**, *115*, 9941−9947.
(32) Huser, T.; Yan, M.; Rothberg, L. J. Single Chain Spectroscopy of Conformational Dependence of Conjugated Polymer Photophysics. *Proc. Natl. Acad. Sci. U. S. A.* **2000**, *97*, 11187−11191.
(33) Hollars, C. W.; Lane, S. M.; Huser, T. Controlled Non-Classical Photon Emission from Single Conjugated Polymer Molecules. *Chem. Phys. Lett.* **2003**, *370*, 393−398.
(34) Habuchi, S.; Onda, S.; Vacha, M. Mapping the Emitting Sites within a Single Conjugated Polymer Molecule. *Chem. Commun.* **2009**, No. 32, 4868−4870.
(35) Park, H.; Hoang, D. T.; Paeng, K.; Kaufman, L. J. Localizing Exciton Recombination Sites in Conformationally Distinct Single Conjugated Polymers by Super-Resolution Fluorescence Imaging. *ACS Nano* **2015**, *9*, 3151−3158.
(36) Feist, F. A.; Tommaseo, G.; Basché, T. Single-Molecule Spectroscopy of MEH-PPV Polymer Molecules in Different Host Matrices. *J. Phys. Chem. C* **2009**, *113*, 11484−11490.
(37) Feist, F. A.; Tommaseo, G.; Basché, T. Observation of Very Narrow Linewidths in the Fluorescence Excitation Spectra of Single Conjugated Polymer Chains at 1.2 K. *Phys. Rev. Lett.* **2007**, *98*, 208301.
(38) Yamagata, H.; Hestand, N. J.; Spano, F. C.; Köhler, A.; Scharsich, C.; Hoffmann, S. T.; Bässler, H. The Red-Phase of Poly[2-Methoxy-5-(2-Ethylhexyloxy)- 1,4-Phenylenevinylene] (MEH-PPV): A Disordered HJ-Aggregate. *J. Chem. Phys.* **2013**, *139*, 114903.
(39) Traiphol, R.; Sanguansat, P.; Srikhirin, T.; Kerdcharoen, T.; Osotchan, T. Spectroscopic Study of Photophysical Change in Collapsed Coils of Conjugated Polymers: Effects of Solvent and Temperature. *Macromolecules* **2006**, *39*, 1165−1172.
(40) Mirzov, O.; Bloem, R.; Hania, P. R.; Thomsson, D.; Lin, H.; Scheblykin, I. G. Polarization Portraits of Single Multichromophoric Systems: Visualizing Conformation and Energy Transfer. *Small* **2009**, *5*, 1877−1888.
(41) Liang, J. J.; White, J. D.; Chen, Y. C.; Wang, C. F.; Hsiang, J. C.; Lim, T. S.; Sun, W. Y.; Hsu, J. H.; Hsu, C. P.; Hayashi, M.; et al. Heterogeneous Energy Landscapes of Individual Luminescent Conjugated Polymers. *Phys. Rev. B: Condens. Matter Mater. Phys.* **2006**, *74*, 1−9.
(42) Park, H.; Hoang, D. T.; Paeng, K.; Yang, J.; Kaufman, L. J. Conformation-Dependent Photostability among and within Single Conjugated Polymers. *Nano Lett.* **2015**, *15*, 7604−7609.
(43) Hu, Z.; Adachi, T.; Haws, R. T.; Shuang, B.; Ono, R. J.; Bielawski, C. W.; Landes, C. F.; Rossky, P. J.; Vanden Bout, D. A. Excitonic Energy Migration in Conjugated Polymers: The Critical Role of Interchain Morphology. *J. Am. Chem. Soc.* **2014**, *136*, 16023−16031.
(44) Hu, Z.; Haws, R. T.; Fei, Z.; Boufflet, P.; Heeney, M.; Rossky, P. J.; Vanden Bout, D. A. Impact of Backbone Fluorination on Nanoscale Morphology and Excitonic Coupling in Polythiophenes. *Proc. Natl. Acad. Sci. U. S. A.* **2017**, *114*, 5113−5118.
(45) Yang, J.; Park, H.; Kaufman, L. J. Highly Anisotropic Conjugated Polymer Aggregates: Preparation and Quantification of Physical and Optical Anisotropy. *J. Phys. Chem. C* **2017**, *121*, 13854−13862.
(46) Yang, J.; Park, H.; Kaufman, L. J. In Situ Optical Imaging of the Growth of Conjugated Polymer Aggregates. *Angew. Chem., Int. Ed.* **2018**, *57*, 1826−1830.
(47) Grey, J. K.; Kim, D. Y.; Norris, B. C.; Miller, W. L.; Barbara, P. F. Size-Dependent Spectroscopic Properties of Conjugated Polymer Nanoparticles. *J. Phys. Chem. B* **2006**, *110*, 25568−25572.
(48) Lin, H.; Hania, P. R.; Bloem, R.; Mirzov, O.; Thomsson, D.; Scheblykin, I. G. Single Chain versus Single Aggregate Spectroscopy of Conjugated Polymers. Where Is the Border? *Phys. Chem. Chem. Phys.* **2010**, *12*, 11770−11777.
(49) Vogelsang, J.; Lupton, J. M. Solvent Vapor Annealing of Single Conjugated Polymer Chains: Building Organic Optoelectronic Materials from the Bottom Up. *J. Phys. Chem. Lett.* **2012**, *3*, 1503−1513.
(50) Traub, M. C.; Vogelsang, J.; Plunkett, K. N.; Nuckolls, C.; Barbara, P. F.; Vanden Bout, D. A. Unmasking Bulk Exciton Traps and Interchain Electronic Interactions with Single Conjugated Polymer Aggregates. *ACS Nano* **2012**, *6*, 523−529.
(51) Stangl, T.; Wilhelm, P.; Remmerssen, K.; Höger, S.; Vogelsang, J.; Lupton, J. M. Mesoscopic Quantum Emitters from Deterministic Aggregates of Conjugated Polymers. *Proc. Natl. Acad. Sci. U. S. A.* **2015**, *112*, E5560−E5566.
(52) Eder, T.; Stangl, T.; Gmelch, M.; Remmerssen, K.; Laux, D.; Höger, S.; Lupton, J. M.; Vogelsang, J. Switching between H- and J-Type Electronic Coupling in Single Conjugated Polymer Aggregates. *Nat. Commun.* **2017**, *8*, 1641.
(53) Steiner, F.; Lupton, J. M.; Vogelsang, J. Role of Triplet-State Shelving in Organic Photovoltaics: Single-Chain Aggregates of Poly(3-Hexylthiophene) versus Mesoscopic Multichain Aggregates. *J. Am. Chem. Soc.* **2017**, *139*, 9787−9790.
(54) Hoang, D. T.; Yang, J.; Paeng, K.; Kwon, Y.; Kweon, O. S.; Kaufman, L. J. In Situ Multi-Modal Monitoring of Solvent Vapor Swelling in Polymer Thin Films. *Rev. Sci. Instrum.* **2016**, *87*, 015106.
(55) Ferdous, S.; Nakaya, M.; Russell, T. P.; Wang, D.; Nakajima, K.; Liu, F.; Muramatsu, A.; Yagihashi, N.; Liang, X. New Insights into Morphology of High Performance BHJ Photovoltaics Revealed by High Resolution AFM. *Nano Lett.* **2014**, *14*, 5727−5732.
(56) Adachi, T.; Lakhwani, G.; Traub, M. C.; Ono, R. J.; Bielawski, C. W.; Barbara, P. F.; Vanden Bout, D. A. Conformational Effect on Energy Transfer in Single Polythiophene Chains. *J. Phys. Chem. B* **2012**, *116*, 9866−9872.
(57) Spano, F. C.; Silva, C. H- and J-Aggregate Behavior in Polymeric Semiconductors. *Annu. Rev. Phys. Chem.* **2014**, *65*, 477−500.
(58) Tenopala-Carmona, F.; Fronk, S.; Bazan, G. C.; Samuel, I. D. W.; Penedo, J. C. Real-Time Observation of Conformational Switching in Single Conjugated Polymer Chains. *Sci. Adv.* **2018**, *4*, No. eaao5786.
(59) Neef, C. J.; Ferraris, J. P. MEH-PPV: Improved Synthetic Procedure and Molecular Weight Control. *Macromolecules* **2000**, *33*, 2311−2314.

DOI: 10.1021/acs.jpcc.9b08075
J. Phys. Chem. C 2019, 123, 29418−29426

(60) Tian, Y.; Sheinin, V.; Kulikova, O.; Mamardashvili, N.; Scheblykin, I. G. Improving Photo-Stability of Conjugated Polymer MEH-PPV Embedded in Solid Matrices by Purification of the Matrix Polymer. *Chem. Phys. Lett.* **2014**, *599*, 142−145.
(61) Park, H.; Kwon, Y.; Kaufman, L. J. Complex Photophysical Behaviors Affect Single Conjugated Molecule Optical Anisotropy Measurements. *J. Phys. Chem. C* **2019**, *123*, 1960−1965.
(62) Sahoo, D.; Tian, Y.; Sforazzini, G.; Anderson, H. L.; Scheblykin, I. G. Photo-Induced Fluorescence Quenching in Conjugated Polymers Dispersed in Solid Matrices at Low Concentration. *J. Mater. Chem. C* **2014**, *2*, 6601−6608.
(63) Ebihara, Y.; Habuchi, S.; Vacha, M. Conformation-Dependent Room-Temperature Emission Spectra of Single MEH-PPV Chains in Different Polymer Matrices. *Chem. Lett.* **2009**, *38*, 1094−1095.
(64) Yu, J.; Hu, D.; Barbara, P. F. Unmasking Electronic Energy Transfer of Conjugated Polymers by Suppression of O2 Quenching. *Science* **2000**, *289*, 1327−1330.
(65) Kim, D. Y.; Grey, J. K.; Barbara, P. F. A Detailed Single Molecule Spectroscopy Study of the Vibronic States and Energy Transfer Pathways of the Conjugated Polymer MEH-PPV. *Synth. Met.* **2006**, *156*, 336−345.
(66) Yu, Z.; Barbara, P. F. Low-Temperature Single-Molecule Spectroscopy of MEH-PPV Conjugated Polymer Molecules. *J. Phys. Chem. B* **2004**, *108*, 11321−11326.
(67) Feist, F. A.; Zickler, M. F.; Basché, T. Origin of the Red Sites and Energy Transfer Rates in Single MEH-PPV Chains at Low Temperature. *ChemPhysChem* **2011**, *12*, 1499−1508.
(68) Collini, E.; Scholes, G. D. Electronic and Vibrational Coherences in Resonance Energy Transfer along MEH-PPV Chains at Room Temperature. *J. Phys. Chem. A* **2009**, *113*, 4223−4241.
(69) Ghosh, A.; Jana, B.; Chakraborty, S.; Maiti, S.; Jana, B.; Ghosh, H. N.; Patra, A. Exciton Dynamics and Formation Mechanism of MEH-PPV Polymer-Based Nanostructures. *J. Phys. Chem. C* **2017**, *121*, 21062−21072.
(70) Köhler, A.; Hoffmann, S. T.; Bässler, H. An Order-Disorder Transition in the Conjugated Polymer MEH-PPV. *J. Am. Chem. Soc.* **2012**, *134*, 11594−11601.
(71) Gaab, K. M.; Bardeen, C. J. Wavelength and Temperature Dependence of the Femtosecond Pump−Probe Anisotropies in the Conjugated Polymer MEH-PPV: Implications for Energy-Transfer Dynamics. *J. Phys. Chem. B* **2004**, *108*, 4619−4626.
(72) Nguyen, T.-Q.; Martini, I. B.; Liu, J.; Schwartz, B. J. Controlling Interchain Interactions in Conjugated Polymers: The Effects of Chain Morphology on Exciton-Exciton Annihilation and Aggregation in MEH-PPV Films. *J. Phys. Chem. B* **2000**, *104*, 237−255.

DOI: 10.1021/acs.jpcc.9b08075
J. Phys. Chem. C 2019, 123, 29418−29426